Numerical simulation of corium flow through rod bundle and/or debris bed geometries with a model based on Lattice Boltzmann method

J. Garcia Sarmiento, Florian Fichot, Vincent Topin, P. Sagaut

Numerical simulation of corium flow through rod bundle and/or debris bed geometries with a model based on Lattice Boltzmann method

Garcia Sarmiento J., Fichot F., Topin V.
IRSN/PSN-RES/SAM, Cadarache, France
Sagaut P.
M2P2, Aix-Marseille Université, France

1 December 2024

Abstract

A new model is proposed to investigate the relocation and the distribution of hot corium flows in different configurations (rod bundle, porous debris bed) representative of a severe accident in a Light Water Reactor (LWR). Our model relies on the coupling between a modified Lattice Boltzmann Method (LBM), called Free-Surface LBM, that solves hydrodynamics of unsaturated corium and a Finite Volume Method (FVM) that solves heat transfers. Corium solidification and melting are addressed by implementing a correlation between the temperature and the viscosity. Several simulations on representative elementary volumes were performed, varying configurations (debris bed, rod bundle with and without grid). From the results, it is possible to capture important details of the flow at a scale lower than the pore scale and, at the same time, it is possible to take into account the average effects at the scale of several pores. Presented as a proof of concept these preliminary studies show the interest of this kind of CFD approach to identify which parameters at microstructure scale can potentially govern the corium relocation kinetics at macroscopic scale. It will provide useful information that might improve core degradation models in severe accident codes, such as ASTEC.

KEYWORDS: lattice Boltzmann method ; nuclear reactor; severe accident ; solidification ; melting ; phase change

1 Introduction

1.1 Severe accidents and corium flows

The studies related to nuclear safety are of great importance as well as immense complexity. From theoretical models to experiments, researchers try to understand the behaviour of the reactor core in case of a severe accident to prevent major complications and potential consequences for the environment. From an experimental viewpoint, a wide database has been built year after year to characterize the different phenomena involved in core degradation. However, predicting their physical couplings and the evolution of the core geometry remain crucial issues that are difficult to study experimentally due to the costs and safety issues related to using prototypical materials at very high temperatures.

Severe Accidents Codes, such as ASTEC [1] [1, 2, 3], developed at IRSN or MELCOR [4] (USNRC-SNL, USA), answer partially this problem. They consist in several modules modeling separate phenomena, coupled together through a common database and solved from a set of local balance equations and transport equations. Validated on real accidents (TMI-2, Fukushima) and experimental databases, these codes are used by plant operators and safety authorities to perform safety studies to predict consequences of potential accidents (as it was done recently for the nuclear power plant at Zaporijia in Ukraine which was under the threat of a military attack). But although severe accident codes are robust and able to provide conservative (or reasonably pessimistic) estimates of the consequences of various scenarios, they give inaccurate estimates of the degradation phase. In fact, physical correlations and material properties are often interpolated to be applied at high temperatures in the ranges where they are not validated; and the geometry of the degraded core, involving corium and debris distribution and relocation, is modeled quite arbitrarily due to the lack of available data.

To date, the models involving the representation and the kinetics of evolution of fragmented and/or melted materials in the core during a severe accident rely mainly on the analysis of two severe accidents (TMI2, 1979 [5, 6] and

[1] Accident Source Term Evaluation Code

Fukushima 2011) and on three major integral test programs: the Phébus-SFD and Phébus-FP neutron-heated experiments and the out-of-pile [7, 8] , electrically heated, CORA [9] and QUENCH [10] experiments. All previous tests provided rich information about the triggering of the degradation, its kinetics, the nature of the mixtures involved, the influence of chemical interactions and the final states morphology. But an accurate description of the evolution of core geometry and influence of the corium distribution on the fluid flow during its progression is still missing.

1.2 Choice of computational model for corium flow

Quite different types of flows may be encountered in the situations of interest, when corium progresses through a rod bundle or a debris bed, under the effect of gravity. Several cases correspond to the "free surface flow" classification: the position of the interface does not depend on the presence of the gas and on surface tension. The case of counter-current flows of gas and corium in a debris bed is more complex and requires to take into account surface tension and density difference. But the occurrence of such case is only possible if the gas flow is not "diverted" around the debris bed. Therefore, in this work, we have considered that a free surface model would be of interest for many situations of corium flow and would be very efficient from a numerical point of view because only the meshes were liquid is present would have to be computed. Similarly, the choice was made to select a Lattice-Boltzman Model (LBM) rather than the resolution of Navier-Stokes equations, as we expected a significant gain in computation time for this kind of flow through porous media where the Reynolds number is not large. LBM is known to be particularly fast and stable for single phase flows, therefore we expected a similar efficiency for a free surface flow. This choice was of course arbitrary be it appeared to be relevant in the end.To our knowledge, it is the first application of LBM in the field of corium flow and severe accidents. An alternative option which is also very efficient from a numerical point of view is the moving particle semi-implicit (MPS) method. It is a macroscopic, deterministic particle method (Lagrangian mesh-free method) developed by Koshizuka and Oka in 1996. The MPS method is used to solve the Navier-Stokes equations in a Lagrangian framework. A fractional step method is applied which consists of splitting each time step in two steps of prediction and correction. The fluid is represented with particles, and the motion of each particle is

calculated based on the interactions with the neighboring particles by means of a kernel function. Convection is directly calculated by the motion of these particles. Thus, numerical diffusion, which is an important problem in finite difference methods, is avoided. The interfaces are always clear even if fragmentation or merging of the continuum occurs. Gradient and Laplacian operators involved in the governing equations are transformed to equivalent particle interactions. This method was developped at the University of Tokyo and initially applied to the difficult problem of corium-water interaction and steam explosion [11]. Later, the method was applied to other issues involving corium because it is convenient to deal efficiently with problems with a moving interface: liquid/gas, liquid/solid or liquid/liquid. And several interfaces of different types can also be managed by the method, through an appropriate colouring of the particles. corium spreading. And later, it was applied to the issue of stratification non miscible liquids [12]. [13] calculated corium spreading over a concrete floor. In this approach, immobilization of the crust is modeled by stopping the solid particle movement only when the particle is in contact with the wall, substrate or any other immobilized particles. Alternatively, the crust may re-melt by the heat from the bulk fluid. As soon as solid fraction of the immobilized particle is below a given threshold, the particle is considered as fluid particle and released to the bulk flow. That last example has many similarities with the cases of interest addressed in this paper. MPS and LBM approaches share the common feature of calculating the local velocity field only from the knowledge of the values in a limited number of neighbouring cells or particles. This is the reason for their numerical efficiency. A review of MPS applications in nuclear engineering is made in [14].

1.3 Choice of options for our LBM approach

Since there is no phase change between liquid and gas and no chemical reaction, it seems that there would be no benefit in using models involving free energy gradient (phase field or Cahn-Hilliard) or density gradient. Such models are quite complex and would not provide a significant improvement of the physical modelling that is necessary for this type of flow. Another kind of model is the so-called "pseudo-potential" model introduced by [15]. It is also designed to deal with phase change and multiple components. It introduces an interaction potential that create attractive or repulsive forces near the interface. This force is expressed by a variation of pressure and is

introduced in the momentum equation. The equation of state $p(\rho)$ is modified in order to become non monotonous. The change of phase occurs in regions where $\frac{dp}{d\rho} < 0$.This model is able to reproduce surface tension effects. Another kind of model was introduced by [16]: it was designed to deal with two non miscible fluids and reproduces surface tension effects. It was initially used for two-phase flow in porous media. This model introduces "colors" for the two phases and follows the motion of each colored "particle". The same idea of "color function" is used in the VOF approach for interface tracking. Therefore, it appears interesting to investigate such model and the possibility to combine it with VOF method. This was already done by several authors [17, 18, 19, 20, 21, 22, 23].

In the present work, we introduce a new (in this context) numerical model to *improve the characterization of the corium geometry and its evolution during the core degradation.* The core is considered locally as a porous medium composed of a liquid phase (corium), a gas phase (steam) and a solid phase (intact and fragmented structures, solidified corium) whose geometry evolves: phase changes (melting or solidification) consecutive to heat transfers between phases (conduction, convection, radiation) or chemical reactions (dissolution, liquefaction...), mechanical degradation (fragmentation) and transfers (corium flows, debris collapses) can impact strongly the porous medium micro-structure and therefore the ensuing degradation. Due to the numerous complex phenomena involved, some simplifications are assumed : we do not consider fragmentation processes (formation of debris); we consider only unfavorable situations in which no water supply is available and steam flow velocity is small, i.e. we *do not account for the influence of the gas phase (steam) on liquid phase (corium) and neglect therefore mechanical influence of steam on corium, which is justified in many situations because* $\rho_{corium} >> \rho_{steam}$*)*; we neglect heat transfer by radiation and we do not model chemical interactions, for the sake of simplicity (but it would not be difficult to add to the model because the interfaces are identified). In this framework we propose a numerical model based on the coupling between a Free Surface Lattice Boltzmann Method (FS-LBM) and Finite Volume Method (FVM) for the numerical simulation of the evolution of molten materials in the degraded core in a nuclear Pressurized Water Reactor (PWR). The Free Surface LBM handles the hydrodynamics of liquid corium flow and the FVM is in charge of the heat transfers in the system (similar approaches can be

found in [24, 25]. The choice of such hybrid approach was made for two reasons: first, the FVM solver was already available in our computational tool and, second, we considered that implementing a convection-diffusion solver using explicitely the LBM mass fluxes would be a generic solution for solving other similar problems like species conservation or passive scalar transport because the equations are similar. Therefore, this hybrid coupling enables further extension of the model, in particular to deal with several species and chemical reactions between them. Phase change processes (solidification or melting) are addressed by implementing a correlation between the temperature and the viscosity. Our numerical choices rely on two main arguments: 1) LBM is by nature a local resolution method that makes it very adapted to high-performance computing on parallel architectures. Although the present work does not involve parallelization, future works will consist in it together with implementation of 3D geometries; 2) FS-LBM, by neglecting the gas, allows to consider fine meshing without penalizing strongly computational time.
In the following we start by the description of the numerical model, involving basic LBM features, Free Surface theory, thermal coupling with FVM and accounting of viscosity variation. In the second part we show, as a proof of concept, simulations results of three test cases whose geometries are typical of a reactor core: vertical rods, with or without obstacle (grids) or debris. By analyzing the simulations results and comparing them with real observations, we demonstrate the qualitative consistency of the model and its potential for future works.

2 Numerical model

2.1 Lattice Boltzmann Model

As an alternative to the conventional Navier-Stokes equations solvers that are based on discretization of macroscopic governing equations, the LBM was developed some decades ago by [26] with a solid physical background based on the mesoscopic kinetic equation (Boltzmann equation), where the description of the flow is made in terms of the probability of finding a particle in a determined state. The basic quantity of the LBM is the discrete-velocity distribution function $f_i(\mathbf{x}, t)$ often called the particle distribution function (DF). Based on Kinetic theory it represents the density of particles with ve-

locity $\mathbf{c}_i = (c_{ix}, c_{iy}, c_{iz})$ at position $\mathbf{x}$ and time t. The macroscopic quantities of the fluid (density ρ and velocity $\mathbf{u}$) are computed from the moments of f:

$$\rho(\mathbf{x}, t) = \sum_i f_i(\mathbf{x}, t) \qquad , \qquad \rho\mathbf{u}(\mathbf{x}, t) = \sum_i \mathbf{c}_i f_i(\mathbf{x}, t) \tag{1}$$

For each node i, $\mathbf{c}_i$ is one of a small discrete set of velocities $\{\mathbf{c}_i\}$ and the points $\mathbf{x}$ define the position on a square lattice in space, with lattice spacing Δx. Additionally, f_i is defined only at discrete times t, separated by a time step Δt. For two-dimensional simulations, nine directions are commonly used ($D2Q9$ model). The directions of the velocity vectors are shown in Figure 1 a). By discretizing the Boltzmann Equation in velocity space, physical space

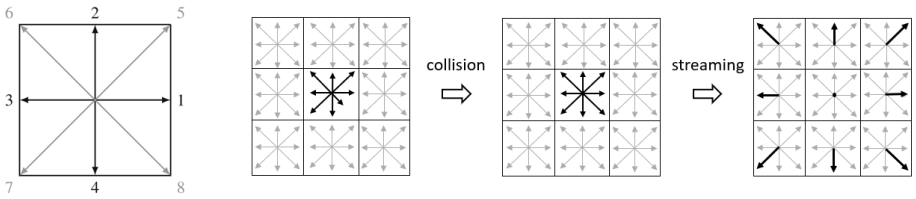

Figure 1: a) D2Q9 velocity scheme; b) Illustration of collision and streaming steps for the populations f_i.

and time we find the lattice Boltzmann equation (LBE):

$$f_i(\mathbf{x} + c_i\Delta t, t + \Delta t) = f_i(\mathbf{x}, t) + \Omega_i(\mathbf{x}, t) \quad . \tag{2}$$

This expresses that particles $f_i(\mathbf{x}, t)$ move with velocity $\mathbf{c}_i$ to a neighbouring point $\mathbf{x} + \mathbf{c}_i\Delta t$ at the next time step $t + \Delta t$. At the same time, particles are affected by a collision operator Ω_i that models particle collisions by redistributing particles among the population f_i at each site. Among the different collision operators Ω_i available, the simplest that can be used for Navier-Stokes simulations is the BGK operator:

$$\Omega_i(f) = -\frac{f_i - f_i^{eq}}{\tau}\Delta t \tag{3}$$

It relaxes the populations towards an equilibrium f_i^{eq} at a rate determined by the relaxation time τ. The equilibrium is given by:

$$f^{eq}(\mathbf{x}, t) = \rho\omega_i \left(1 + \frac{\mathbf{c}_i \cdot \mathbf{u}}{c_s^2} + \frac{(\mathbf{c}_i \cdot \mathbf{u})^2}{2c_s^4} - \frac{|\mathbf{u}|^2}{2c_s^2}\right) \quad , \tag{4}$$

where ω_i is the set of weights associated to each velocity, $\mathbf{u}$ represents the macroscopic flow velocity and $\mathbf{c}_i$ corresponds to the set of unitary velocities. The sets of values ω_i and $\mathbf{c}_i$ for $D2Q9$ scheme are given in table 1. Equation

Table 1: Explicit values for the lattice weights ω_i, and velocities $\mathbf{c}_i$ for $D2Q9$ scheme.

Direction i	ω_i	$\mathbf{c}_i$
0	$4/9$	$(0,0)$
$1-4$	$1/9$	$(\pm1,0)$, $(\pm1,0)$
$5-8$	$1/36$	$(\pm1,0)$, $(\pm1,0)$

(2) reproduces the Navier-Stokes equations (NSE) for an isothermal ideal gas in the limit of low-density fluctuations and low Mach numbers ([27, 28]) in the continuous limit of infinitely small cells. The link between the LBE and the NSE can be determined using the Chapman-Enskog analysis ([29]). The kinematic shear viscosity is given by the relaxation time τ as:

$$\nu = c_s^2 \left(\tau - \frac{\Delta t}{2} \right). \tag{5}$$

with c_s a constant representing the isothermal speed of sound on the lattice network. In case of $D2Q9$ scheme, $c_s = 1/\sqrt{3}$.

The LBM algorithm proceeds in two steps – the collision and the streaming. The collision is simply an algebraic local operation: from the density ρ and macroscopic velocity $\mathbf{u}$ are computed the equilibrium distributions f_i^{eq} and the post-collision distribution f_i^*. Then the streaming step propagates the resulting distribution f_i^* to neighbouring nodes. When these two operations are completed, time step is finished and operations are repeated. The collision and streaming steps for the D2Q9 velocity set are summarized in Figure 1 b).

No-slip boundary conditions for the LBM are implemented by reflecting the DFs at the boundary and at interfaces with solid obstacles. Hence for each cell, instead of copying the neighboring DF from a boundary cell during streaming, its own opposing DF is taken. This results in zero normal and tangential velocities along the boundary (see [29]).

2.2 Free Surface method

The Free Surface Lattice Boltzmann Method (FS-LBM) emerges as an alternative to simulate multi-phase flows with a high density ratio [21, 30]. Based on the VOF approach, it relies on the description of the interface evolution between two different fluids where one predominates and determines the hydrodynamics and the other one can be neglected. Three types of cells are identified based on their liquid volume fraction ϕ: Fluid cells $\phi = 1$, Gas cells $\phi = 0$ and ϕ for Interface cells can vary from 0 to 1. The value of ϕ determines the cell flag C used to distinguish liquid cells ($C = 1$), liquid-gas interface cells ($C = 0.5$) and gas cells ($C = 0.$). In the case of a porous medium two additional values for cell flag are introduced; $C = 2.0$ for solid cells and $C = 1.5$ for solid-liquid interface cells .
Similarly to VOF approach, the main idea of the Free Surface Method is to evaluate mass fluxes between cells at each time step in order to calculate new masses in cells and new liquid volume fractions ϕ. From ϕ, we obtain a new map for cell flags C. Given that in LBM the DFs carry information about the amount of particles at a certain position that moves in the i direction, it is obvious that the streaming step leads to mass advection between neighbor cells. For a cell at position x, the new mass M at time $t + \Delta t$ relies on the contributions in all directions such as:

$$M(x, t + \Delta t) = M(\mathbf{x}, t) + \sum_i m_i(\mathbf{x}, t) \quad , \tag{6}$$

where m_i is the mass contribution on direction i considering the outgoing and incoming populations. Some special attention needs to be paid to the flag of the involved cells since the volume fraction determines the contact area between the cells. To achieve this, a coefficient α is defined for each pair of cells so the mass increment is given by:

$$m_i(\mathbf{x}, t) = \alpha_i[f^*_{\bar{i}}(\mathbf{x} + \mathbf{c}_i\Delta t, t) - f^*_i(\mathbf{x}, t)] \quad , \tag{7}$$

where the subscript $\bar{i}$ stands for the opposite direction of i and the superscript $*$ for the post-collision populations. The values of α_i vary from 0 to 1 and involve the volume fraction value when two interface cells are considered (See Table 2). One of the main advantages of Free Surface Method stands in the fact that gas cells are neglected and consequently not calculated. It implies the reconstruction of some f_i's coming from the gas during the streaming

Table 2: Mass exchange coefficient for different types of cells.

Cell	**Neighbor**	α_i
gas	Gas	0
	Interface	0
Interface	Gas	0
	Interface	$\frac{1}{2}[\phi(\mathbf{x}) + \phi(\mathbf{x} + \mathbf{c}_i\Delta t)]$
	Liquid	1
Liquid	Interface	1
	Liquid	1

step. To do so, the pressure p_s at interface determining the value for ρ_s is used to compute the equilibrium function such that :

$$\rho_s = \frac{p_s}{c_s^2} \text{ and } f_i(\mathbf{x}, t) = f_i^{eq}(\rho_s, \mathbf{u}) + f_{\bar{i}}^{eq}(\rho_s, \mathbf{u}) - f_{\bar{i}}(\mathbf{x}, t) \quad , \tag{8}$$

where $\bar{i}$ stands for the opposite direction of i and the velocity $\mathbf{u}$ is taken as the value on the interface cell.

At this step it is possible to impose surface tension effects at the interface introducing $\kappa(\mathbf{x}, t)$ the local curvature and σ the constant surface tension of the liquid. The modified expression for the pressure is therefore written as:

$$p_s' = p_s + 2\sigma\kappa(\mathbf{x}, t) \quad . \tag{9}$$

and the curvature is computed in terms of the divergence of the normal vector $\hat{\mathbf{n}}$ at the interface as

$$\kappa = -(\nabla \cdot \hat{\mathbf{n}}). \tag{10}$$

The volume fraction is then obtained using $M = \phi\rho V_{cell}$ where ρ is the liquid density and V_{cell} is the cell volume. Evolution of cell flags is done according to the volume fraction at each of them. It should be noted that only a few transitions are allowed in order to preserve the continuity of the interface. In other words, a liquid cell can not be next to a gas one and there must be an interface cell in between to allow the mass exchange and therefore the flag change. These changes are only performed at interface cells that can be either filled or emptied, making the cell flag change to fluid or gas, respectively. Once the new gas and fluid cells are defined, it is necessary to

guarantee the continuity of the interface. To do so, a loop on these modified cells is performed and takes the information about the neighbors flag. For filled cells it will search for gas neighbors and will change their status to interface. Similarly, for an empty cell, the fluid neighbors will be marked as interface, thus ensuring the continuity of the interface.
For each flag change in a cell, it is necessary to pay attention to the excess of mass remaining in the cell and to redistribute it among the interface neighbor cells. In such cases, the mass is distributed in the direction of the interface motion using the normal vector at the interface. The absence of calculation in the gas domain is expected to massively save computational time but also to avoid difficulty of dealing with large density ratio in multi-phase models [30]. We did not quantify it in the present study but it has to be noted that the thermal resolution (see section 2.3) is performed on the whole domain, including gas cells. More details about the mass redistribution process are available in [30].

2.3 Thermal coupling

The energy conservation equation, expressed with the enthalpy as main variable, is solved using a Finite Volumes (FV) method implemented in CALIF^{3}S software. Enthalpy of the gas is neglected and we need to account both liquid and solid part in the cell. It is assumed that solid and liquid have the same temperature (thermal equilibrium assumption) and that the liquid volume fraction x_l is a monotonically increasing function of temperature T: $x_l = f_l(T)$. The enthalpy is written as the sum of enthalpies of liquid and solid parts:

$$h(T) = (1 - x_l)h_s(T) + x_l h_l(T) \tag{11}$$

in which each contribution (liquid or solid) can be expressed from heat capacity Cp and solidification enthalpy Δh:

$$h_s(T) = CpT \tag{12}$$

$$h_l(T) = \Delta h + CpT \tag{13}$$

Therefore we have:

$$h(T) = CpT + x_l \Delta h \tag{14}$$

and

$$\nabla h = Cp\nabla T + \Delta h \nabla x_l \tag{15}$$

The algorithm of resolution of the free surface model ensures the conservation of total mass of fluid thanks to a mass redistribution (normalisation) process (see section 2.2). As a consequence, the divergence of the mass flux is not necessarily zero, especially in the cells within or near the interface:

$$\frac{\partial \rho\phi}{\partial t} \neq 0 \tag{16}$$

For convenience the mass in a cell represented by $\rho\phi$ is denoted $\tilde{\rho}$. At each time step we store the local value of mass variation for fluid cells

$$\dot{\rho}_{fl} = \frac{\partial \tilde{\rho}}{\partial t} + \nabla \cdot (\tilde{\rho}\mathbf{u}) \tag{17}$$

and interface cells:

$$\dot{\tilde{\rho}}_{int} = (\frac{\partial \tilde{\rho}}{\partial t})_{norm} \tag{18}$$

We note $\dot{\tilde{\rho}}_{tot} = \dot{\rho}_{fl} + \dot{\tilde{\rho}}_{int}$. This term is used in the energy conservation. Starting from the conservative form of the enthalpy conservation:

$$\frac{\partial(\tilde{\rho}h)}{\partial t} + \nabla \cdot (\tilde{\rho}h\mathbf{u}) = \nabla \cdot (-k\nabla T) + \dot{Q} \tag{19}$$

we develop it in order to exhibit the mass variation:

$$h\frac{\partial \tilde{\rho}}{\partial t} + h\nabla \cdot (\tilde{\rho}\mathbf{u}) + \tilde{\rho}\frac{\partial h}{\partial t} + \tilde{\rho}\mathbf{u}.\nabla h = \nabla \cdot (-k\nabla T) + \dot{Q} \quad . \tag{20}$$

We can replace the mass variation and obtain an equation for the time variation of temperature:

$$\tilde{\rho}Cp\frac{\partial T}{\partial t} = \nabla \cdot (-k\nabla T) - \tilde{\rho}Cp\mathbf{u}.\nabla T - \tilde{\rho}\Delta h\mathbf{u}.\nabla x_l + \dot{Q} - h\dot{\tilde{\rho}}_{tot} \tag{21}$$

Equation 21 is solved by a standard Finite Volume solver.

In our 2D case, a regular square meshing coinciding with the LBM D2Q9 network is defined. Each cell of the FV meshing includes 9 nodes of the LBM grid. On the FV meshing, the density ρ^{FV} is defined at the center of each cell like ρ^{LBM} in LBM meshing, such that for each node i we have $\rho_i^{FV} = \rho_i^{LBM}$. On the contrary, there is no straightforward correspondence between FV velocities (defined at faces) and LBM velocities (defined at cell

centers). The FV velocity value $\mathbf{u}_{ij}^{FV}$ at interface of each couple of FV cells (i, j) is computed from LBM velocity values such as :

$$\mathbf{u}_{ij}^{FV} = \frac{1}{2}(\mathbf{u}_i^{LBM} + \mathbf{u}_j^{LBM}).\mathbf{n}_{ij} \tag{22}$$

where $\mathbf{n}_{ij}$ corresponds to the normal vector to the face between cells i and j.

Since the gas phase is not considered in the Free Surface LBM, we impose its density $\rho_g^{FV} = 10^{-4}\rho_l^{FV}$ and velocity $\mathbf{u}_g^{FV} = 0.$ in the FV resolution. To avoid loss of energy through the gas phase during heat transfer resolution, it is also necessary to impose a small diffusivity k_g such that $k_l >> k_g$ and to define a specific heat capacity Cp that depends on the volume fraction of liquid α such that:

$$k_g = 10^{-6}k_l \qquad \text{(arbitrary to keep energy within liquid phase)}, \tag{23}$$

$$Cp = \alpha Cp_l + (1-\alpha)Cp_g \quad . \tag{24}$$

2.4 High viscosity flows and variable viscosity

The temperature field obtained from the coupling with the finite volume method is returned to LBM Free surface to manage the viscosity of fluid and solid cells, and consequently to model melting/solidification processes. The coexistence in the same domain of high viscosity ratios (solid/liquid) can lead to some instabilities or lack of accuracy. Therefore, this issue requires some strategy to improve the performance: in this case we implement a modification of the LBM collision kernel, known as the "Two Relaxation Times" (TRT) model [31]. The TRT scheme relies on the principle that any lattice quantity ψ_i can be decomposed into two components, one symmetric and the other anti-symmetric. This leads to the construction of the TRT model, where the evolution is driven by two relaxation times: τ^+ and τ^-. The parameter τ^+ is directly related with the kinematic viscosity and the other can be freely adjusted accordingly to find the stability of the model through a so-called **magic parameter** Λ given by

$$\Lambda = \left(\tau^+ - \frac{1}{2}\right)\left(\tau^- - \frac{1}{2}\right) \quad . \tag{25}$$

A recommended choice is $\Lambda = 1/4$ [29]. For any value of τ^+, one can always select the free parameter τ^- such that $\Lambda = 1/4$. The TRT model is implemented similarly to the BGK model, using the same form for the equilibrium

functions and velocity schemes. The TRT Boltzmann equation reads:

$$\frac{\partial f_i}{\partial t} + \frac{\partial}{\partial x_\alpha}(c_{i,\alpha}) = -\frac{1}{\tau^+}(f_i^+ - f_i^{eq+}) - \frac{1}{\tau^-}(f_i^- - f_i^{eq-}) \quad , \tag{26}$$

where f_i^+ and f_i^- are the symmetric and anti-symmetric components of the distribution functions f_i, expressed as:

$$f_i^+ = \frac{1}{2}(f_i + f_{\bar{i}}) \qquad ; \qquad f_i^- = \frac{1}{2}(f_i - f_{\bar{i}}), \tag{27}$$

with the index $\bar{i}$ defining the opposite direction of i, i.e. $\mathbf{c}_{\bar{i}} = -\mathbf{c}_i$. Similarly, for the equilibrium function we have:

$$f_i^{eq+} = \frac{1}{2}(f_i^{eq} + f_{\bar{i}}^{eq}) \qquad ; \qquad f_i^{eq-} = \frac{1}{2}(f_i^{eq} - f_{\bar{i}}^{eq}) \qquad , \tag{28}$$

where the equilibrium function is the same used in the standard BGK LBM (see equation 4).

Due to the flexibility and stability provided by the use of two relaxation times in the TRT kernel, it is possible to reach higher values for the viscosity (related to τ^+) and tune accordingly τ^-. In thermal flows, it is common to find a strong dependence on the temperature through the fluid viscosity [32]. This can be treated appropriately by considering a local viscosity at each lattice node. The connection with the lattice Boltzmann method can be seen as a change of the relaxation time, which leads us to define it locally as a function of the temperature field.

We define a dimensionless temperature denoted by θ in terms of the temperature T, defined as:

$$\theta = \frac{T - T_{sol}}{T_{liq} - T_{sol}} \quad , \tag{29}$$

where T_{sol} is the solidus temperature and T_{liq} is the liquidus temperature. The relation between the temperature and the viscosity is given in Equation 30 as a piecewise function, where there are two intervals defining the different phases with a constant viscosity, and an intermediate region where the viscosity varies with the temperature.

$$\nu(T) = \begin{cases} \nu_{liq} & \text{if } \theta \leq 1 \\ \min\left(\nu_{max}, \theta^{-3}\nu_{liq}\right) & \text{if } 0 < \theta < 1 \\ \nu_{max} & \text{if } \theta \leq 0 \end{cases} \quad , \tag{30}$$

where we chose $\nu_{max} = 1000\nu_{liq}$ for this work.

To catch melting and solidification processes the cell flag C is changed according to the value of viscosity on the cell : a liquid cell is changed to solid cell when $\nu > \nu_{max}$ and a solid cell is changed to liquid when $\nu \leq \nu_{max}$.

2.5 Validation

Several validations tests were carried out to check the ability of the model to reproduce theoretical / experimental results. As summarized in table 3, the model shows a good behavior in different configurations, ranging from simple isothermal and thermal flows (Poiseuille, lid cavity, steady-state freezing) to multiphasic system submitted to gravity (Dam-break). More details are available about these validation tests in [33].

Table 3: Examples of validation tests performed with Free-Surface LBM in 2 dimensions.

Configuration	Description	Remarks
Poiseuille Flow	Pressure gradient imposed for different Re, BGK and TRT operators	Retrieves parabolic profile for velocity.
LID Driven Cavity	$Re = 100, 400, 100$, BGK collision operator.	Vertical and horizontal velocities consistent with [34].
Dam-Break	TRT collision operator, gravity	Evolution of the water front consistent with [35].
Steady-state freezing	2D channel with cooling conditions on wall.	Evolution of the solid layer thickness (formation of ice) consistent with [36].

3 Application to the flow of a molten material in porous media with a temperature difference

3.1 Dimensionless analysis

This section presents results of numerical simulations representative of different states encountered during the degradation of a core reactor. The aim is to show the ability of the model to catch some physical features as "a proof of concept". As it can be seen in figure 2, a degraded core presents large zones of molten materials and debris beds, sometimes mixed together, and that can be relocated at lower elevations through still intact fuel rods and grids. To simplify we can consider the flow of corium in two borderline configurations : 1) through a set of intact fuel rods (bundle configuration) ; 2) through a debris bed (porous configuration). In each configuration, it

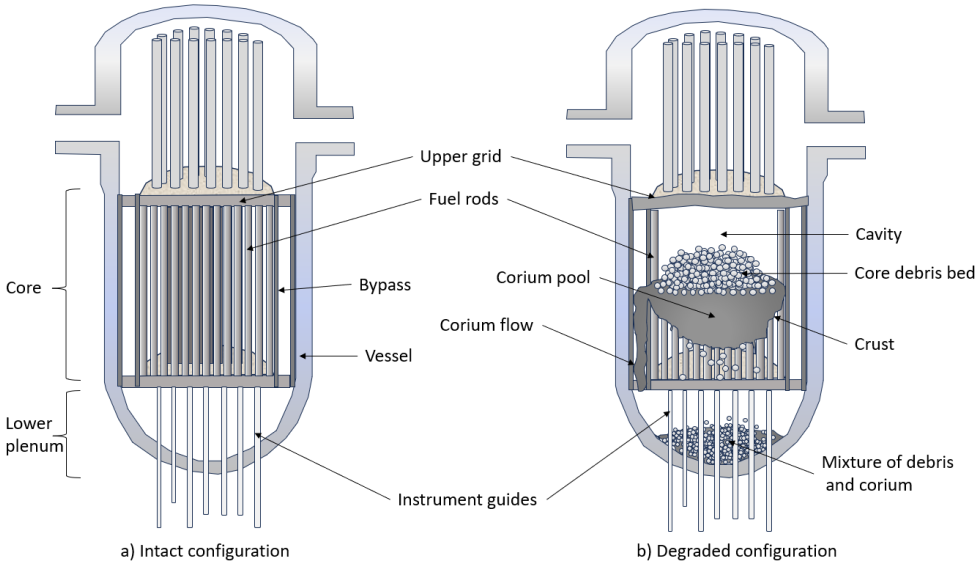

Figure 2: Schematic representation of a PWR core reactor. a) intact; b) degraded

is possible to characterize the corium flow by estimating some dimensionless numbers :

- The Reynolds number Re spans between 10 (flow through a porous

medium in a dense debris bed configuration) and more than 10000 (free fall between fuels rods),

- the Capillary number Ca, estimated between 1.10^{-5} and 1.10^{-3} depending corium velocity,
- the Bond number Bo, is between 0.15 and 1.3 depending on the pores size,
- the Weber number We is between 1.10^{-2} (porous configuration) and 5.10^{3} (bundle configuration).

In presence of a debris bed (porous configuration) the flow is therefore expected to be inertial with a non-negligible role of surface tension compared viscous forces and gravity. On the contrary, between fuel rods (bundle configuration) the flow is expected to be turbulent and the surface tension plays a minor role.

The above dimensionless analysis should be however put in perspective taking into account that it relies on an isothermal progression of corium assumption, which is not exactly the case during a core degradation. In fact melting and solidification processes obviously occurring in such configuration participate to a strong geometry evolution that can either slow down or accelerate the corium flow.

3.2 Modeling

In the following we propose here to investigate two simple configurations in which a mixture of molten materials (corium) relocates either in a bundle of rods or in a debris bed. We consider a 2D rectangular domain of width $L_x = 6 \times 10^{-2}$m and height $L_y = 10^{-1}$ m, delimited by two walls on the left and right sides. Inside this domain, we define 3 rectangular solid walls of width $L_{rod} = 0.01$ m separated by a distance $L_{gap} = 0.005$ m (those walls represent fuel rods). Three cases are considered: 1) configuration without grid; 2) configuration with grids, represented by squares located at an elevation $H_{grid} = 2.5 \times 10^{-2}$ m; 3) configuration with a debris bed. In the last case, a python pre-processing was made to generate a sample of 60 squares of random size (between $2.4mm$ and $9mm$) and random position, creating a domain with a mean porosity equal to 0.77. The obtained porosity is greater

than the one expected in a dense debris bed (around 0.42 in 3D, [37]). However we note that a 2D geometry requires a greater porosity to keep the coalescence of the void phase. In that context the last configuration, without representing a real debris bed (2D representation), is proposed to evaluate the model behavior in presence of a disordered porous medium.
The upper part of the fuel rods is defined as initially melted by imposing a temperature $T_{hot} = 3000$ K on a length $H_{melt} = 3 \times 10^{-2}$ m. All other solids are set initially at a temperature $T_{ini} = T_{cold} = 2600$ K, including debris. The top part of the domain is set adiabatic and a fixed temperature $T_{cold} = 2600$ K is imposed at the bottom, left and right sides during the whole simulation. In terms of velocity, a no-slip condition is applied on all boundaries. Figure 3 a) illustrates the simulation configurations. The densities of solid

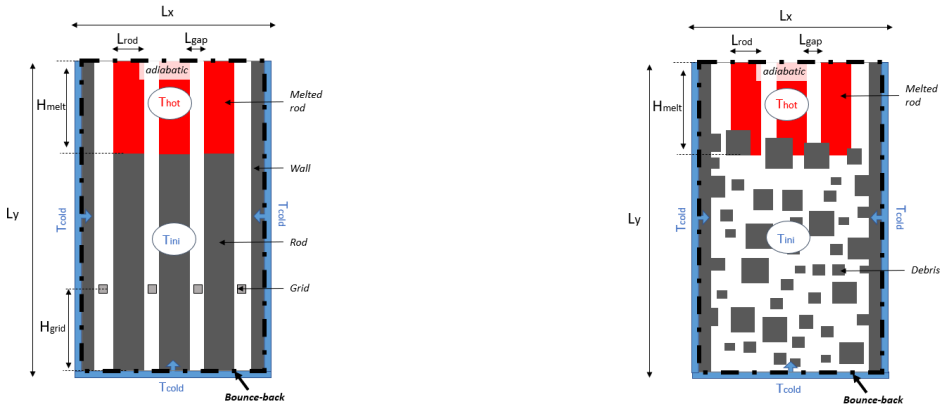

(a) Configuration with fuel rods

(b) Configuration with debris

Figure 3: Schematic representation of test-cases configurations a) with parallel fuel rods; b) with debris.

and liquid are defined equal to the density of corium $\rho = 8.0 \times 10^3$ kg/m^3 and the dynamic viscosity for liquid (molten parts) is set to $\mu = 6.0 \times 10^{-3}$ Pa s, corresponding to a kinematic viscosity $\nu = 0.75 \times 10^{-6}$m^2/s.
To simplify the temperature resolution, the specific heat of all components has been set to $C_p = C_{pl} = C_{pg} = 1$ J kg^{-1}K^{-1}, the solid and liquid diffusivity to $k_l = 0.1$ m^{2}s^{-1} and the gas diffusivity arbitrary to $k_g = 10^{-6} k_l$. Temperatures of liquefaction T_{liq} and solidification T_{sol} have been fixed to 2750 K and 2700 K, respectively. In term of LBM resolution, applying a real gravity imposes small time steps and fine meshing. In order to reduce the computational

cost, the reduced gravity $g = 0.05\text{m/s}^2$ has been imposed along the vertical direction and the surface tension has been set to $\sigma = 0.5 \times 10^{-3}\text{kg/s}^2$. The computational domain has been meshed with $N_x = 100$ lattice nodes along x and $N_y = 167$ nodes along y, corresponding to cell size of $\Delta x = 6 \times 10^{-4}$ m. Considering a free fall velocity and a reference porous length $L_{gap} = 5\text{mm}$, we obtain $Re \simeq 1.10^4$, $Ca \simeq 1.2$, $Bo \simeq 20$ and $We \simeq 1.5.10^4$. We note that these values, which are partly induced by numerical aspects in this first "proof of concept" code version, are relatively far from the values estimated in the previous analysis concerning the influence of surface tension compared to viscous drag forces and gravity. By neglecting surface tension effects, we focus here mainly on phase change (solidification and melting) processes that are expected to influence strongly the corium pool formation and relocation. It is however important to note that using a reduced gravity obviously induces a complexity to interpret results, due to the fact that impact of fast relocation is neglected.
We point out here that the proposed configurations do not claim to represent real reactor configurations but rather evaluate the model behavior under controlled geometry and boundaries conditions. In fact, several limitations (2D, absence of radiative exchanges, absence of oxidation, etc) prevent direct comparison to realistic situations. However, we note that some choices concerning the geometry and the temperatures range look like well-known experiments such as PHEBUS [38], CORA [9] or CORDEB [39]. In particular for the debris configuration, the dimensions of the domain and the cold thermal conditions on walls are relatively close to the CORDEB experiments (Rasplav facility), in which a corium was heated and molten by induction in a water cooled crucible of about $7cm$ internal diameter. In fact the CD4 and CD5 series focused on the conditions in which a heated molten steel would be able to penetrate within a debris bed by varying steel temperature between $1850°C$ and $2300°C$.

3.3 Results

3.3.1 Bundle configuration without grid

In this first configuration, we can observe the qualitative behaviour predicted by the model for the flow of a large mass of super-heated liquid through cold parallel channels. One of the interesting points to observe in Figure 4 is the coexistence of two modes of relocation:

- The first one consists of small drops or rivulets which flow rather fast and are able to reach low elevations, or even flow out of the domain. This corresponds to a relocation mode already observed in experiments of fuel rods degradation such as CORA by [9]. In this paper, the authors indicate that, when the cladding material melts "*the melt relocates along the surface as rivulets (candling) and, to a minor extent, as droplets (free fall), i.e. without contact with other surfaces. Film flow type of melt relocation down the rods was not observed.*".

- The second one consists of a massive and compact pool of liquid which goes down slowly. The reason for this slow progression is the presence of a partly solidified crust below the liquid pool (clearly visible on the right image of Figure 5 with a rather thick zone of high-viscosity material): this crust successively remelts and refreezes, depending on the balance between heat lost along the walls and heat gained from the overlying liquid pool. In the same paper, [9] indicate that, when the fuel melts (i.e. a much larger mass of liquid is involved), "*larger amounts of molten material are produced so that the blockage zone in the lower bundle region is clearly larger. The formation of a distinct crust consisting of metallic material was observed, on which the metallic and ceramic melts formed later accumulated*"

This double-relocation process was also described, from the analysis of PHEBUS bundle tests ([38]) by [40] who formulate it as follows: "*Rapid processes of drop- or rivulet-like income from above and outcome to below take place against the background of the slow relocation of the molten mass (slug). This slow relocation makes the main contribution to the axial mass transfer and correlates with the downward propagation of the high-temperature front*".
Looking at the final distribution of porosity (or, equivalently, of mass) shown in Figure 5 d), we see that the "liquid pool" zone is completely full (no porosity) and that there is an almost linear gradient of porosity from the pool towards the bottom where the porosity is almost equal to its initial value. The gradient is caused by the presence of the rivulets. This kind of profile may be compared to measurements of mass profile made in the PHEBUS-FP experiments ([38]).
Finally, we see that the model, with the physical properties that were chosen for this calculation, is able to reproduce those experimental observations. It is particularly interesting because current volume-averaged models are not able to distinguish between the fast relocation process (which is mainly driven

by gravity and inertia) and the slow relocation process (which is mainly governed by the thermal balance at the leading edge of the relocation front).

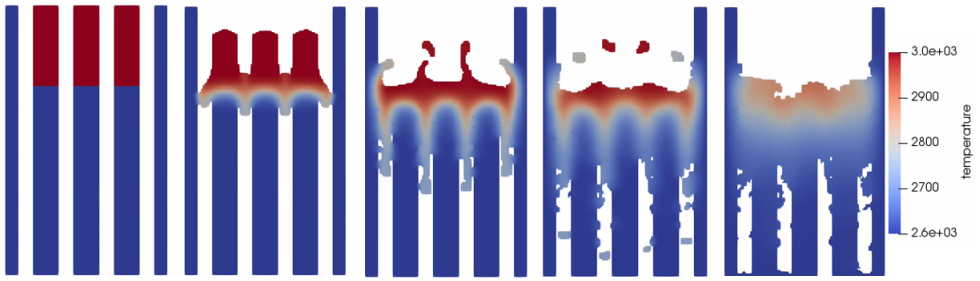

Figure 4: Simulation of a magma flow through fuel rods at times $0s, 0.6s, 1.2s, 1.6s, 3.2s$, respectively. Temperature is represented in color levels.

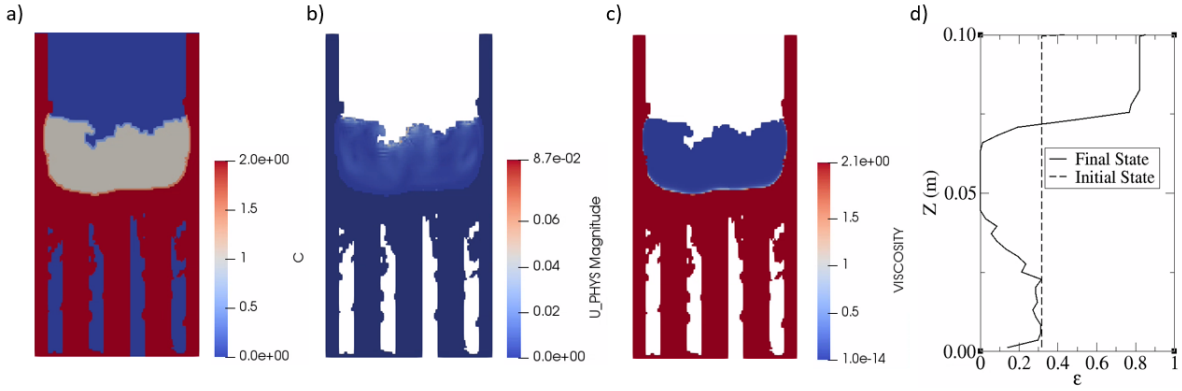

Figure 5: Final state of simulation with fuel rods: a) phase index (0=gas, 0.5=interface gas/liquid, 1=liquid, 1.5=interface liquid/solid, 2=solid); b) velocity (m/s); c) kinematic viscosity in lattice units. d) Porosity profile at initial and final states for simulation with fuel rods.

3.3.2 Bundle configuration with grids

When we look at the same configuration with the addition of a "grid", we can observe in Figure 6 that the rivulets are not able to go below the grid.

This is mainly due to the increase of heat transfer with the cold surfaces (which are doubled at the location of the grid) but also to the decrease of velocity (or increase of friction) when arriving at the grid. As a result, solidification takes place when the liquid reaches the grid. This corresponds to an expected behaviour which had already been observed experimentally: in [9], the authors indicate that "*the lower, colder grid spacers act as 'material catcher" for solid and liquid bundle components and thus exert a major influence on the development of cooling channel blockages (crusts)*". Of course, the blockage of the flow depends on the size of the grid, on the superheat of the liquid and the temperature of the walls. However, we did not perform a sensitivity analysis because in this simulation some thermal properties are different from the real ones, like the gravity. Therefore, the quantitative behaviour cannot be strictly interpreted for those first simulations.
Another interesting result is the formation of closed porosities, as can be observed in the last (down-right) image of Figure 6 and in the porosity profile in Figure 6 d). Such porosities might have an important effect on the coolability of corium in case of water injection: open porosities are favorable for water penetration and cooling whereas closed porosities have no impact on the permeability of the resulting corium configuration.

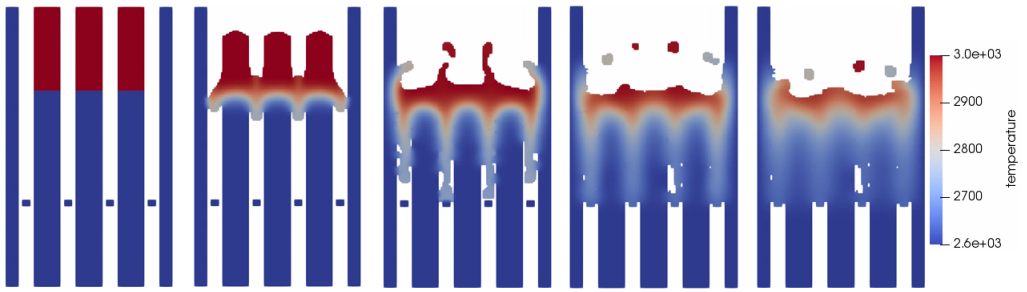

Figure 6: Simulation of a magma flow through fuel rods with grids at times 0s, 0.6s, 1.2s, 1.6s, 2s, respectively. Temperature is represented in color levels.

3.3.3 Debris bed configuration

In this last case where the hot liquid flows through a random arrangement of cold squares, it is interesting to observe that the propagation is initially quite random (see the bottom left image of Figure 8) but it finally reaches a rather symmetrical shape (see the bottom right image of Figure 8 and Figures 9).

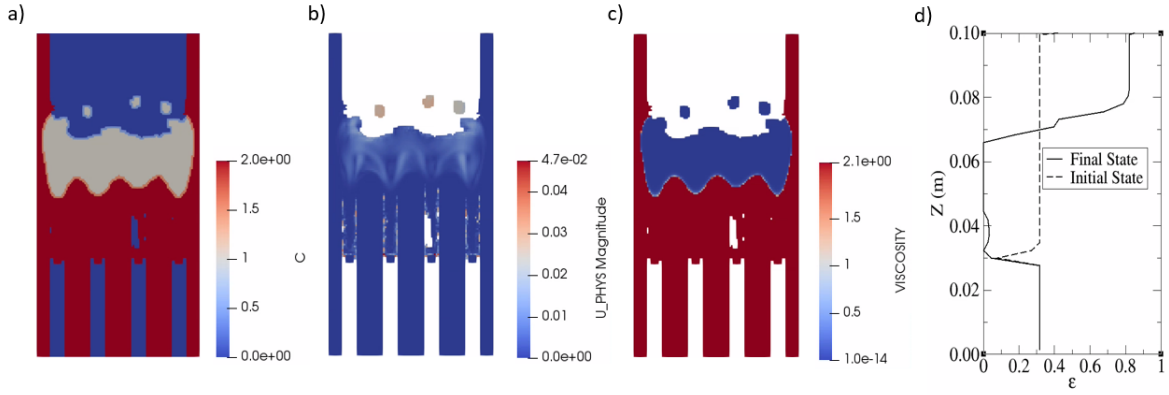

Figure 7: Final state of simulation with fuel rods and grids: a) phase index (0=gas, 0.5=interface gas/liquid, 1=liquid, 1.5=interface liquid/solid, 2=solid); b) velocity (m/s); c) kinematic viscosity in lattice units; d) Porosity profile at initial and final states for simulation with fuel rods and grids.

This can also be observed on the porosity profiles (see Figure 9 d)): starting from an initial state with many fluctuations in the porosity, we finally obtain a profile very close to those observed in bundle configurations (see Figures 4 d) and 7 d)). This shows that the heat transfers govern the progression and that the symmetry of the system (in terms of temperature) is not lost because of the random arrangement, as soon as the liquid has passed through several "lines" of obstacles. This can also be explained, looking at the right image of Figure 9, by the build-up of a lateral crust, originating from the wall at the top and progressing towards the centre at lower elevations. The presence of this crust causes an accumulation of liquid towards the center. This type of propagation has already been observed in experiments like CORDEB, as illustrated in Figure 10.The CORDEB program studied corium phenomena taking place at different stages of molten pool formation in the reactor vessel. It addressed particularly the issue of molten steel progression across an oxide debris bed (see [39]).

4 Conclusions

The initial motivation for this work was to investigate the potential of a Lattice Boltzmann method (LBM) as a proof of concept to describe the flow

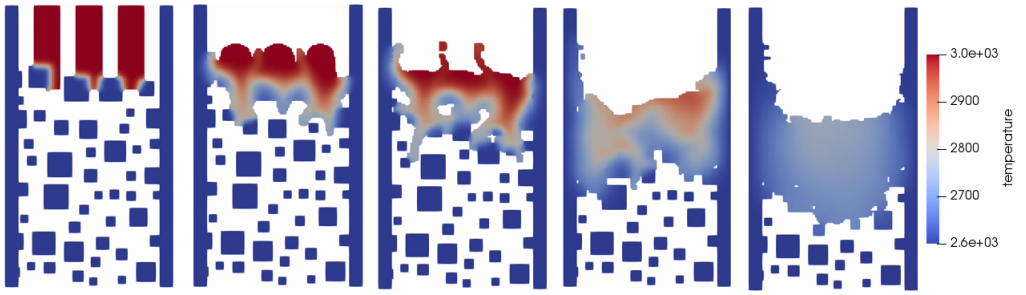

Figure 8: Simulation of a magma flow through a debris bed at times $0s, 0.75s, 1s, 2s, 10s$, respectively. Color is assigned according to the value of temperature.

of a molten material through a reactor core geometry, at different stages of degradation. The expected benefit of the LBM approach was the gain of computational time compared to the usual Navier-Stokes resolution methods. This led us to choose a Free Surface LBM model where only the liquid distribution functions are calculated and the gas flow is not calculated. The algorithm uses some elements of the Volume-of-Fluid (VOF) method and ensures the conservation of mass. It is a sharp interface type model in the sense that only one mesh is necessary to make a geometrical reconstruction of the transition between liquid and gas, as it has already been done with classical computational fluid methods such as in [41]. Similar coupled LBM/VOF approaches have been extensively described by previous authors, such as [23]. In the flows considered in this work, it is expected that solidification may take place at some location where the solid elements are colder or that the solid elements may melt when they get in contact with hot liquid. Therefore, it was necessary to estimate the temperature of the liquid and solid phases. This is made by solving the energy equation with a standard finite volume solver, over a meshing that is directly deduced from the LBM lattice. An additional energy source term must be introduced as a correction in the energy conservation because the divergence of the velocity field obtained after the LBM resolution is not exactly zero. As a result, the coupled LBM/FV model ensures the mass and energy conservation. The temperature field is used to increase the viscosity when temperature is lower than the melting temperature. This results in a decrease of the relaxation time in the collision function. However, because the LBM resolution is less accurate when the relaxation time is large, we have chosen to replace the standard BGK kernel

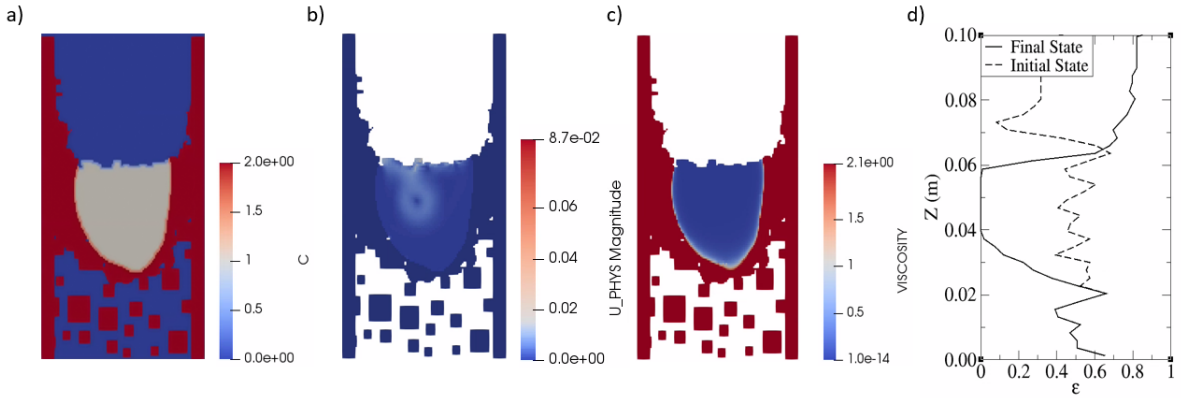

Figure 9: Final state of simulation with debris: a) phase index (0=gas, 0.5=interface gas/liquid, 1=liquid, 1.5=interface liquid/solid, 2=solid); b) velocity (m/s); c) kinematic viscosity (m^2/s); d) Porosity profile at initial and final states for simulation with debris.

by a Two Relaxation Times (TRT) kernel which avoids this limitation. In the end, the model differs significantly from the basic LBM models for single phase flows. At this point of development, the model is able to deal with the configurations of interest described in the introduction. With the sufficient number of meshes, it is possible to capture important details of the flow at a scale smaller than the pore scale and, at the same time, it is possible to take into account the average effects at the scale of several pores. The numerical efficiency is such that we will consider, in the near future, much larger computation domains or 3D applications. One of the main advantages of the present implementation is that the hydrodynamics is solved only in the nodes where the liquid phase is present during the LBM evolution.
The presented model, which aimed at investigating the potential of Lattice Boltzmann method to describe the flow of a molten material in nuclear context, is the first step to reach a more complete modeling. A crucial coming development is the 3D representation without which a quantitative comparison with real geometries is not possible. In that perspective, the parallelization of the code is required to be able to account large number of cells, together with higher Reynolds numbers (i.e. using real gravity and viscosity) implying smaller time steps. In addition, a regularization algorithm should be helpful to keep reasonable computational times, as mention in [30]. An example of a 3D simulation including parallelization and Hermite regularization algorithm

Figure 10: Cross section obtained after progression of molten steel through a debris bed (CORDEB CD5-03) test [39].

performed with an under-development version of the code is shown in figure 11. In the future, more complex configurations such as debris beds previously computed by a granular method in [37] could be considered. Further devel-

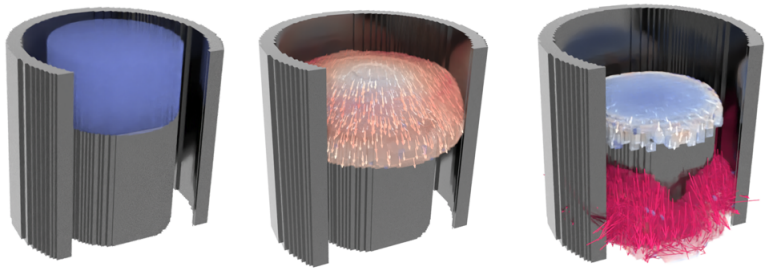

Figure 11: Example of 3D simulation of an isothermal flow of a partially molten pellet inside a cladding. Liquid velocity is represented in color level. Under-development version of 3D-parallelized Free-Surface LBM.

opments are also needed to improve the thermal resolution, in particular the heat transfers through the gas phase which are not perfectly controlled with the chosen approach. Radiative heat transfers in the gas phase, neglected here but crucial for a comprehensive core degradation modeling, should be also accounted to provide quantitative results. One solution envisaged would be to replace the thermal FV resolution by a fully LBM one, considering for example models mentioned in [42]. We should also look at the possibility to consider more accurate laws for viscosity and surface tension which have been voluntarily chosen simple. Finally, we need to make a more quantitative validation of the model for the cases where surface tension governs the progression.

ACKNOWLEDGMENTS

We thank our IRSN colleagues F. Babik, R. Monod, F. Duval and J.-C. Latché for their valuable help.

References

[1] P. Chatelard, L. Laborde, Astec v2.2 code validation: Illustrative results and main outcomes, Nuclear Engineering and Design 413 (2023) 112547. doi:https://doi.org/10.1016/j.nucengdes.2023.112547.
URL https://www.sciencedirect.com/science/article/pii/S0029549323003965

[2] J. Zambaux, L. Laborde, Interfacial heat transfer with non-condensable gas in astec v2.2: Application to severe accidents study during pwr cold shutdown states, Nuclear Engineering and Design 411 (2023) 112434. doi:https://doi.org/10.1016/j.nucengdes.2023.112434.
URL https://www.sciencedirect.com/science/article/pii/S0029549323002832

[3] I. Gómez-García-Toraño, L. Laborde, F. Fichot, H. Mutelle, Reflooding of degraded cores in astec v2.1: Modelling and validation on pearl experiments, Nuclear Engineering and Design 393 (2022) 111768. doi:https://doi.org/10.1016/j.nucengdes.2022.111768.
URL https://www.sciencedirect.com/science/article/pii/S0029549322001224

[4] L. L. Humphries, V. G. Figueroa, M. F. Young, D. Louie, J. T. Reynolds, Melcor computer code manuals, Tech. rep., Sandia National Lab.(SNL-NM), Albuquerque, NM (United States) (2015).

[5] D. W. Akers, R. K. Mccardell, M. L. Russell, G. Worku, Tmi-2 core materials and fission product inventory, Nuclear Engineering and Design 118 (3) (1990) 451–461. doi:https://doi.org/10.1016/0029-5493(90)90046-Z.

[6] R. K. McCardell, M. L. Russell, D. W. Akers, C. S. Olsen, Summary of tmi-2 core sample examinations, Nuclear Engineering and Design 118 (3) (1990) 441–449. doi:https://doi.org/10.1016/0029-5493(90)90045-Y.

[7] B. Clément, R. Zeyen, The objectives of the phebus fp experimental programme and main findings, Annals of Nuclear En-

ergy 61 (2013) 4–10, special Issue : Phebus FP Final Seminar. doi:https://doi.org/10.1016/j.anucene.2013.03.037.

[8] M. Barrachin, O. de Luze, T. Haste, G. Repetto, Late phase fuel degradation in the phebus fp tests, Annals of Nuclear Energy 61 (2013) 36–53, special Issue : Phebus FP Final Seminar. doi:https://doi.org/10.1016/j.anucene.2013.03.041.

[9] P. Hofmann, S. J. L. Hagen, V. Noack, G. Schanz, L. K. Sepold, Chemical-physical behavior of light water reactor core components tested under severe reactor accident conditions in the cora facility, Nuclear Technology 118 (3) (1997) 200–224. doi:https://doi.org/10.13182/NT118-200.

[10] M. Steinbrück, M. Große, L. Sepold, J. Stuckert, Synopsis and outcome of the QUENCH experimental program, Nuclear Engineering and Design 240 (7) (2010) 1714–1727. doi:10.1016/j.nucengdes.2010.03.021.

[11] S. Koshizuka, H. Ikeda, Y. Oka, Numerical analysis of fragmentation mechanisms in vapor explosions, Nuclear Engineering and Design 189 (1) (1999) 423–433. doi:10.1016/S0029-5493(98)00270-2.

[12] G. Li, Y. Oka, M. Furuya, M. Kondo, Experiments and MPS analysis of stratification behavior of two immiscible fluids, Nuclear Engineering and Design 265 (2013) 210–221. doi:10.1016/j.nucengdes.2013.09.006.
URL http://dx.doi.org/10.1016/j.nucengdes.2013.09.006

[13] Y. Yasumura, A. Yamaji, M. Furuya, Y. Ohishi, G. Duan, Investigation on influence of crust formation on VULCANO VE-U7 corium spreading with MPS method, Annals of Nuclear Energy 107 (2017) 119–127. doi:10.1016/j.anucene.2017.04.002.
URL http://dx.doi.org/10.1016/j.anucene.2017.04.002

[14] W. Li, X. Liang, J. Lin, P. Guo, Q. Ma, Z. Dong, J. Liu, Z. Song, H. Wang, Numerical simulation of ship oil spill in arctic icy waters, Applied Sciences (Switzerland) 10 (2 2020). doi:10.3390/app10041394.

[15] X. Shan, H. Chen, Lattice boltzmann model for simulating flows with multi phases and components, Physical Review E 47 (1993) 1815–1819. doi:10.1103/PhysRevE.

[16] A. K. Gunstensen, D. H. Rothman, S. Zaleski, G. Zanetti, Lattice boltzmann model of immiscible fluids, Physical Review A 43 (1991) 4320–4327. doi:10.1103/PhysRevA.43.4320.

[17] J. Tölke, M. Krafczyk, M. Schulz, E. Rank, Lattice boltzmann simulations of binary fluid flow through porous media, Philosophical Transactions of the Royal Society A: Mathematical, Physical and Engineering Sciences 360 (2002) 535–545. doi:10.1098/rsta.2001.0944.

[18] C. Körner, M. Thies, T. Hofmann, N. Thürey, U. Rüde, Lattice boltzmann model for free surface flow for modeling foaming, Journal of Statistical Physics 121 (2005) 179–196. doi:10.1007/s10955-005-8879-8.

[19] J. Tölke, S. Freudiger, M. Krafczyk, An adaptive scheme using hierarchical grids for lattice Boltzmann multi-phase flow simulations, Computers and Fluids 35 (2006) 820–830. doi:10.1016/j.compfluid.2005.08.010.

[20] N. Thürey, T. Pohl, U. Rüde, M. Öchsner, C. Körner, Optimization and stabilization of lbm free surface flow simulations using adaptive parameterization, Computers and Fluids 35 (2006) 934–939. doi:10.1016/j.compfluid.2005.06.009.

[21] N. Thürey, Physically based animation of free surface flows with the lattice boltzmann method, Ph.D. thesis, Universität Erlangen-Nürnberg (2007).

[22] C. Janssen, M. Krafczyk, A lattice boltzmann approach for free-surface-flow simulations on non-uniform block-structured grids, Computers and Mathematics with Applications 59 (7) (2010) 2215–2235, mesoscopic Methods in Engineering and Science. doi:https://doi.org/10.1016/j.camwa.2009.08.064.

[23] C. F. Janßen, S. T. Grilli, M. Krafczyk, On enhanced non-linear free surface flow simulations with a hybrid lbm-vof model, Computers and Mathematics with Applications 65 (2013) 211–229. doi:10.1016/j.camwa.2012.05.012.

[24] P. LALLEMAND, L.-S. LUO, Hybrid finite-difference thermal lattice boltzmann equation, International Journal of Modern Physics B 17 (01n02) (2003) 41–47. arXiv:https://doi.org/10.1142/S0217979203017060,

doi:10.1142/S0217979203017060.
URL https://doi.org/10.1142/S0217979203017060

[25] Y. Feng, P. Boivin, J. Jacob, P. Sagaut, Hybrid recursive regularized lattice boltzmann simulation of humid air with application to meteorological flows, Physical Review E 100 (8 2019). doi:10.1103/PhysRevE.100.023304.

[26] G. R. McNamara, G. Zanetti, Use of the boltzmann equation to simulate lattice-gas automata, Phys. Rev. Lett. 61 (1988) 2332–2335. doi:10.1103/PhysRevLett.61.2332.

[27] Q. Zou, S. Hou, S. Chen, G. D. Doolen, An improved incompressible lattice boltzmann model for time-independent flows, Journal of Statistical Physics 81 (1995). doi:https://doi.org/10.1007/BF02179966.

[28] X. He, L.-S. Luo, Theory of the lattice boltzmann method: From the boltzmann equation to the lattice boltzmann equation, Phys. Rev. E 56 (1997) 6811–6817. doi:https://doi.org/10.1103/PhysRevE.56.6811.

[29] T. Krüger, H. Kusumaatmaja, O. Shardt, A. Kuzmin, E. M. Viggen, G. Silva, The Lattice Boltzmann Method Principles and Practice, Springer, 2017. doi:10.1007/978-3-319-44649-3.

[30] W. Cao, Investigation of the applicability of the lattice boltzmann method to free-surface hydrodynamic problems in marine engineering, Ph.D. thesis, Université Bretagne Loire (2019).
URL https://tel.archives-ouvertes.fr/tel-02383174

[31] I. Ginzburg, F. Verhaeghe, D. d'Humieres, Two-relaxation-time lattice boltzmann scheme: About parametrization, velocity, pressure and mixed boundary conditions, Communications in computational physics 3 (2) (2008) 427–478.

[32] Z. Guo, T. S. Zhao, Lattice boltzmann simulation of natural convection with viscosity in a porous cavity, Mechanical Engineering 5 (2005) 110–117.

[33] J. Garcia Sarmiento, Characterization of magma flows through a debris bed during a severe accident, Ph.D. thesis, Université Aix-Marseille

(2022).
URL http://www.theses.fr/2022AIXM0445

[34] U. Ghia, K. N. Ghia, C. T. Shin, High-re solutions for incompressible flow using the navier-stokes equations and a multigrid method, Journal of Computational Physics 48 (1982) 387–411.

[35] J. C. Martin, W. Moyce, W. G. Penney, A. T. Price, C. K. Thornhill, Part iv. an experimental study of the collapse of liquid columns on a rigid horizontal plane, Philosophical Transactions of the Royal Society of London. Series A, Mathematical and Physical Sciences 244 (1952) 312 – 324.

[36] Y. Kikuchi, Y. Shigemasa, A. Oe, T. Ogata, Steady-state freezing of liquids in laminar flow between two parallel plates, Journal of Nuclear Science and Technology 23 (11) (1986) 979–991.

[37] D. H. Nguyen, F. Fichot, V. Topin, Investigation of the structure of debris beds formed from fuel rods fragmentation, Nuclear Engineering and Design 313 (2017) 96–107. doi:10.1016/j.nucengdes.2016.11.019.

[38] T. Haste, M. Barrachin, B. Clément, A. Grégoire, N. Girault, M. Laurie, O. D. Luze, P. March, F. Payot, G. Repetto, PSN-RES/SAG/2012-00018: Synthesis of the Phébus FP programme experimental results, Tech. rep., IRSN (2012).

[39] E. Krushinov, Final report : Investigation of interaction between molten stainless steel and the debris in the oxidising atmosphere, TASK 5 (CORDEB 1), Tech. rep., NITI (2015).

[40] M. S. Veshchunov, V. E. Shestak, Model for melt blockage (slug) relocation and physico-chemical interactions during core degradation under severe accident conditions, Nuclear Engineering and Design 238 (12) (2008) 3500–3507. doi:10.1016/j.nucengdes.2008.08.012.

[41] M. Sussman, K. Smith, M. Hussaini, M. Ohta, R. Zhi-Wei, A sharp interface method for incompressible two-phase flows, Journal of Computational Physics 221 (2) (2007) 469–505. doi:https://doi.org/10.1016/j.jcp.2006.06.020.
URL https://www.sciencedirect.com/science/article/pii/S0021999106002981

[42] Y. Wei, X. Liu, K. Zhu, Y. Huang, A unified lattice boltzmann framework for combined radiation-conduction heat transfer, International Journal of Heat and Mass Transfer 200 (2023) 123513. doi:https://doi.org/10.1016/j.ijheatmasstransfer.2022.123513.
URL https://www.sciencedirect.com/science/article/pii/S0017931022009826